Reversible Redox Control of Optoelectronic Properties of Hexagonal Tungsten Oxide Epitaxial Films Grown on YSZ Solid Electrolyte

Gowoon Kim[a]*, Hai Jun Cho[b], and Hiromichi Ohta[b]*

[a] *Graduate School of Information Science and Technology, Hokkaido University, N14W9, Kita, Sapporo 060-0814, Japan*

[b] *Research Institute for Electronic Science, Hokkaido University, N20W10, Kita, Sapporo 001-0020, Japan*

*Email: woom93@gmail.com, hiromichi.ohta@es.hokudai.ac.jp

KEYWORDS: electrochemical control, Redox reaction, optoelectronic properties, tungsten oxide, WO_3, epitaxial film, YSZ, solid electrolyte

ABSTRACT: Controlling the oxygen concentration in metal oxides is one of the most effective ways to modulate their optoelectronic properties. However, such redox control is difficult for metal oxide epitaxial films due to serious damages induced to the lattice, especially around the film / substrate interface during the large volume change upon the redox treatment. For overcoming this problem, the use of metal oxides with a stress-resistant crystal structure can be effective. Here we show a reversible redox control in the

optoelectronic properties of hexagonal tungsten oxide (h-WO_x) epitaxial films with honeycomb structure. We fabricated highly *c*-axis oriented h-WO_x epitaxial films on (111) yttria-stabilized zirconia (YSZ) single crystal substrate. Upon electrochemical redox treatment at 300 °C with the application of ±3 V to the YSZ solid electrolyte, the oxygen content x of h-WO_x was reversibly controlled in the range of $2.93 \leq x \leq 2.99$ without inducing damage to the crystal lattice. Simultaneously, the electrical conductivity was controlled from ~400 S cm^{-1} to an insulator, and the optical transmission at 1.5 μm in wavelength was controlled in the range of 35 − 70%. The present results would be useful for developing metal oxide epitaxial film-based electrochemical optoelectronic devices.

INTRODUCTION

Advanced memory devices that store optoelectronic property changes would be in extremely high demand in near future because of the explosive amount of information to be processed in the upcoming fourth industrial revolution.[1-4] In this regard, many transition metal oxides (TMOs) can be considered as the promising candidate materials of advanced memory devices since the optoelectronic properties of TMOs can be modulated by controlling the oxygen concentration.[5-7] The valence state of TM ions is versatile in a TMO lattice due to their strong ionicity, and several TMOs show crystallographic phase transition upon reduction or oxidation due to the difference in the ionic radius of TM ions before and after the redox reaction. Thus, controlling the oxygen concentration in metal oxides is one of the most effective ways of modulating their optoelectronic properties.

However, such redox control is difficult to apply for metal oxide epitaxial films since it induces serious damage to the crystal lattice, particularly near the film/substrate interface due to the large volume change during the redox treatment. Generally, TMO thin films are grown heteroepitaxially on oxide single crystal substrates with a lattice mismatch.[8] Therefore, the crystal lattice of the TMO thin film is highly strained at the heterointerface between the film and the substrate if the film is thin and not relaxed. If such strained crystal lattice is exposed to some stress, the crystal lattice is easily fractured into pieces. For example, VO_2 epitaxial films grown on lattice-mismatched TiO_2 substrate brakes into tiny pieces upon insulator-to-metal transition.[9, 10]

To overcome this problem, we hypothesized that the use of metal oxides exhibiting a stress-resistant crystal structure would be effective. In this study, we focused on hexagonal tungsten oxide (h-WO_x) epitaxial films for three reasons. First, h-WO_x crystal is composed of honeycomb layers with periodic holes stacked along the *c*-axis [11, 12], and honeycomb structure is known as one of the strongest lattices against stress.[13, 14] Second, *c*-axis oriented h-WO_x crystal can be grown heteroepitaxially on (111) yttria-stabilized zirconia (YSZ) single crystal substrate.[15, 16] Thus, the one-dimensional tunnels are periodically aligned along the growth direction. Third, YSZ substrate can be used as an oxide-ion conducting solid electrolyte. By using YSZ substrate as the solid electrolyte, reversible electrochemical redox control of oxygen contents in $SrCoO_{2.5}$[17-19] and $SrFeO_{2.5}$[20] has been demonstrated

thus far. In this research, we choose h-WO_x epitaxial film grown on (111) YSZ substrate from these points of view.

Here we show reversible redox control of optoelectronic properties of *c*-axis oriented h-WO_x epitaxial films grown on (111) YSZ single crystal substrate. Upon electrochemical redox treatment at 300 °C by applying ±3 V to the YSZ solid electrolyte, the oxygen content x of h-WO_x was reversibly controlled in the range of $2.93 \leq x \leq 2.99$ without inducing any damage to the crystal lattice. Simultaneously, the electrical conductivity was controlled from ~400 S cm^{-1} to an insulator, and the optical transmission at 1500 nm in wavelength was controlled in the range of 35 − 70%. The present results would be of great value in developing metal oxide epitaxial films-based electrochemical optoelectronic devices.

EXPERIMENTAL SECTION

Epitaxial growth of highly *c*-axis oriented h-WO_x films

Highly *c*-axis oriented h-WO_x epitaxial films were heteroeptiaxially grown on (111) YSZ substrate by pulsed laser deposition (PLD, KrF excimer laser, ~0.3 J cm^{-2} $pulse^{-1}$, 10 Hz) technique at a substrate temperature of 500 °C under oxygen atmosphere (2 − 6 Pa). The growth rate was ~8.7 pm $pulse^{-1}$. Details of our PLD condition has been published elsewhere.[21, 22] Heteroepitaxial growth was confirmed using high-energy electron

diffraction (RHEED) after finishing the film growth. The film thickness and orientation were analyzed by high-resolution X-ray diffraction (HRXRD, Cu $K\alpha_1$, λ = 1.54059 Å, ATX-G, Rigaku Co.). Pendellösung fringes in the out-of-plane Bragg diffraction patterns were used to measure the thickness of the resultant h-WO_x epitaxial films. The valence states of W of the resultant h-WO_x epitaxial films were measured by X-ray photoelectron spectroscopy (XPS). We used Al Kα radiation (1486.6 eV) to generate the photoelectrons while using a flood gun to prevent surface charge accumulation. The W 4f (30 − 40 eV) core-level spectra were collected, and the x in WO_x was determined as following.[5]

$$x = \frac{[W^{6+}] \times 3 + [W^{5+}] \times 2.5}{[W^{6+}] + [W^{5+}]}$$

Electrochemical redox treatment

Figure 1(a) shows the schematic illustration of the electrochemical redox treatment. Atomic arrangement of the top view of h-WO_3 film is schematically shown in Figure 1(b). First, the film surface was mechanically pressed on an Al foil (ground electrode). Then, we pasted small amount of Ag paste on the back side of the YSZ substrate. After that the sample was heated at 300 °C in air. We applied a gate voltage (V_G) of −3 V to the Ag electrode for 10 min (Figure 1(c) upper). After this oxidation treatment, the film was fully oxidized. Then, we electrochemically reduced the film by applying V_G of +3 V for 5 to 200 s (Figure 1(c) lower and Figure S1). The electron density (Q) was calculated by $Q = \int I(t)\, dt$, where I is current and t is time. Then, the x in WO_x was measured by XPS as described above (Figure 1(d) and Figure S2).

Characterization of electrochemically oxidized/reduced h-WO_x epitaxial films

Optical transmission spectra of the h-WO_x films were measured using an ultraviolet-visible-near-infrared spectrometer (UV-vis-NIR, SolidSpec-3700, Shimadzu Co.) and Fourier-transform infrared spectrometer (FT-IR, IRPrestige-21, Shimadzu Co.) at room temperature (RT). Electrical conductivity (σ) was measured by dc four-probe method with van der Pauw electrode configuration from RT to 20 K. Thermopower (S) was measured by steady-state method. Temperature difference (ΔT) and thermoelectromotive force (ΔV) were measured simultaneously at RT, and the S values were calculated from the linear slope of $\Delta T - \Delta V$ plots.

RESULTS AND DISCUSSION

Figure 2(a) (upper) shows the XPS spectrum of the as-grown epitaxial film. The XPS spectrum is composed of W^{6+} and W^{5+}, and the value of x is 2.938. Figure 2(b) (upper) shows the out-of-plane XRD pattern of as-grown h-$WO_{2.938}$ epitaxial film. An intense diffraction peak of 0002 h-WO_x is observed with 111 YSZ substrate. Around the 0002 h-$WO_{2.938}$ diffraction peak, Pendellösung fringes are clearly seen, indicating strong c-axis orientation in the film. From the Pendellösung fringes, the film thickness was calculated to be ~42 nm. Then, the film was electrochemically oxidized at 300 °C in air. Figure 2(a) (lower) shows the XPS spectrum of oxidized h-WO_x. The XPS spectrum became sharper and the W^{5+} peak almost disappeared. The composition of oxidized h-WO_x (namely Oxi 1)

was changed into 2.993 by the electrochemical oxidation. Figure 2(b) (lower) shows the out-of-plane XRD pattern of Oxi 1 h-$WO_{2.993}$. The diffraction peak position of h-$WO_{2.993}$ shifted to smaller scattering vector side due to the *c*-axis lattice expansion from 0.758 to 0.769 nm upon oxidation. It should be noted that Pendellösung fringes are clearly observed after the oxidation treatment, indicating that the oxidation treatment did not affect the *c*-axis orientation of the film. This suggests that the crystal lattice was not damaged despite rather large lattice expansions.

Next, we reduced the Oxi 1 sample electrochemically. We prepared 8 samples with varying chemical compositions from h-$WO_{2.987}$ to h-$WO_{2.931}$. Figure 2(c) summarizes the out-of-plane XRD patterns of the electrochemically reduced samples (linear scale). The peak position of 0002 h-WO_x almost unchanged after the reduction from $x = 2.987$ to $x = 2.981$, while it gradually shifted to higher scattering vector side from $x = 2.981$ to $x = 2.931$ indicating that reversible redox reaction of h-WO_x succeeded. This behavior of the *c*-axis is opposite as compared to other metal oxides, which show lattice expansion upon reduction. Presumably, the inter-atomic repulsion along *c*-axis is suppressed due to the 1D atomic defect tunnel structure. The *c*-axis lattice parameter almost returned to 0.762 nm, which is close to that of the as-grown sample.

Next, we measured the electron transport properties of the electrochemically reduced h-WO_x epitaxial films. Figures 3(a) and 3(b) show the electrical conductivity (σ), and the

thermopower (S) measured at RT. For comparison, data for the PLD-grown h-WO_x films with various oxygen contents of x is also plotted with a grey solid line (Figures 3(a) and 3(b)). The crystallographic analyses of the PLD-grown films are shown in Figures S3−S5. It should be noted that the data of the electrochemical redox treatment was almost perfectly reproduced that of the PLD-grown films. The σ increases from ~0.2 (A) to ~400 S cm^{-1} (H) with decreasing x. Since $|S|$ decreased with increasing σ, carrier concentration increased with decreasing x. Thus, the carrier concentration of h-WO_x was successfully controlled by the electrochemical redox treatment.

Then, we measured the $\sigma - T$ curves of electrochemically reduced h-WO_x epitaxial films in the range of 20 − 300 K. All films showed semiconductor-like behavior of σ; where the σ increased with temperature. The slope of $\sigma - T$ curves gradually decreased with decreasing x. The activation energy (E_a) of the σ around RT decreased from ~212 meV (A) to ~33 meV (H) with decreasing x (Table S1). The decreasing tendency of E_a for the electrochemically reduced h-WOx films is consistent with that of the PLD-grown h-WO_x films (Table S2). These results clearly suggest that carrier concentration was systematically controlled by the electrochemical reduction treatment, and the crystal lattice of h-WO_x film was not destroyed during the process.

Next, we investigated the optical properties. Figure 4(a) shows the optical transmission spectra of the h-WO_x epitaxial films with various reduction states (as-oxidized: Oxi 1, A, E,

and G) from the electrochemical reduction treatments. The spectra of as-grown sample and (111) YSZ substrate are also plotted for comparison. Although the bandgap of YSZ is ~4 eV, the optical transmission of (111) YSZ substrate is only ~75% in the range of 0.4 – 6 μm in wavelength; reflection of YSZ in the range of 0.4 – 6 μm in wavelength is large (~23 %) due to its high refractive index. Compared to the transmission spectrum of YSZ substrate, the Oxi 1 sample shows slightly lower transmission due to an absorption peaking around 1.5 μm in wavelength. The absorption peak intensity gradually increased with oxygen reduction, indicating free carrier absorption. Finally, the optical transmission spectrum of the reduced sample G became similar to that of as-grown sample. Figure 4(b) plots change in the transmission at 1.5 μm in wavelength as a function of x in WO_x. For comparison, data for the PLD-grown h-WO_x films with various oxygen content x (Figure S6) is also plotted with grey solid line. The transmission increased with oxidation and decreased with reduction. The control in the optical transmission control at 1.5 μm in wavelength is clearly demonstrated in the range of 35 − 70%.

Finally, we repeated the electrochemical redox treatment to check the cyclability. Figures 5(a) and 5(b) show the σ and optical transmission at 1.5 μm in wavelength of the redox-treated h-WO_x epitaxial films. Upon reversible electrochemical redox treatment, the σ is controlled from ~300 to ~0.1 S cm^{-1}, and the optical transmission at 1.5 μm in wavelength is controlled in the range of 35 − 70% (Figure S7). Also, surface morphology was not changed during electrochemical redox treatment while keeping less than 0.5 nm of root

mean square roughness (Figure S8). These results indicate an excellent cyclability and stability.

The results we present here demonstrate that our electrochemically redox treatment did not cause serious structural damage to the crystalline lattice of h-WO_x with stress-resistant honeycomb lattice. The optoelectronic properties of h-WO_x were repeatedly controlled electrochemically. The present results would be of great use in the development of metal oxide epitaxial films-based electrochemical optoelectronic devices.

CONCLUSIONS

In summary, we showed reversible redox control in the optoelectronic properties of hexagonal tungsten oxide (h-WO_x) with honeycomb structure epitaxial films. We fabricated highly *c*-axis oriented h-WO_x epitaxial films on (111) YSZ single crystal substrate. Upon electrochemical redox treatment at 300 °C with the application of ±3 V to the YSZ solid electrolyte, the oxygen content x in h-WO_x was reversibly controlled in the range of $2.93 \leq x \leq 2.99$ without inducing damage to the crystal lattice. Simultaneously, the electrical conductivity was controlled from ~400 S cm^{-1} to an insulator, and the optical transmission at 1500 nm in wavelength was controlled between 35% and 70%. The present results would be useful for developing electrochemical optoelectronic devices based on metal oxide epitaxial films.

ASSOCIATED CONTENT

Supporting Information

Supporting Information is available free of charge via the Internet at https://pubs.acs.org/doi/10.1021/acsaem.XXXXXXX.

Transmission at 1.5 μm (T) and the activation energy (E_a) of the electrochemically reduced/oxidized h-WO_x films; T and E_a of the PLD-grown h-WO_x films; time dependence of the current density during the electrochemical reduction treatment while applying +3 V to YSZ substrate; XPS spectra around W 4f peaks of the electrochemically redox treated h-WO_x epitaxial films; change in the out-of-plane XRD patterns of PLD-grown h-WO_x epitaxial films under various oxygen pressure from 2 to 6 Pa during the film growth; comparison of the crystallographic feature of the PLD-grown h-WO_x epitaxial films under oxygen pressure of 6 Pa and 2 Pa; XPS spectra around W 4f peaks of PLD-grown h-WO_x epitaxial films under various oxygen pressure from 2 to 6 Pa during the film growth; optical transmission and photographs of PLD-grown h-WO_x epitaxial films under various oxygen pressure from 2 to 6 Pa during the film growth; changes in the optical transmission spectra of the h-WO_x epitaxial film after repeated electrochemical redox treatment.

AUTHOR INFORMATION

Corresponding Authors

Gowoon Kim − Graduate School of Information Science and Technology, Hokkaido University, N14W9, Kita, Sapporo 060-0814, Japan

ORCiD: orcid.org/0000-0002-5803-839X

Email: woom93@gmail.com

Hiromichi Ohta − Research Institute for Electronic Science, Hokkaido University, N20W10, Kita, Sapporo 001-0020, Japan

ORCiD: orcid.org/0000-0001-7013-0343

Email: hiromichi.ohta@es.hokudai.ac.jp

Author

Hai Jun Cho − Research Institute for Electronic Science, Hokkaido University, N20W10, Kita, Sapporo 001-0020, Japan

ORCiD: orcid.org/0000-0002-8642-4183

Author Contributions

G.K. and H.O. performed the sample preparation and measurements. H.J.C. measured the XPS spectra of the films. G.K. and H.O. planned and supervised the project. All authors discussed the results and commented on the manuscript.

Funding Sources

Hiromichi Ohta received founding from Grants-in-Aid of the JSPS (19H05791). Gowoon Kim received funding from Grants-in-Aid for JSPS Fellows (20J14755).

Notes

The authors declare no competing financial interest.

ACKNOWLEDGEMENTS

This research was supported by Grants-in-Aid for Innovative Areas (19H05791) from the JSPS. G.K. was supported by Grants-in-Aid for JSPS Fellows (20J14755) from the JSPS. A part of this work was supported by Dynamic Alliance for Open Innovation Bridging Human, Environment, and Materials, and by the Network Joint Research Center for Materials and Devices.

REFERENCES

(1) Hwang, C. S.; Dieny, B., Advanced memory—Materials for a new era of information technology. *MRS Bull.* **2018,** *43*, 330-333.

(2) Huang, W.; Yin, L.; Wang, F.; Cheng, R.; Wang, Z.; Sendeku, M. G.; Wang, J.; Li, N.; Yao, Y.; Yang, X., Multibit Optoelectronic Memory in Top‐Floating‐Gated van der Waals Heterostructures. *Adv. Funct. Mater.* **2019,** *29*, 1902890.

(3) Tan, H.; Liu, G.; Zhu, X.; Yang, H.; Chen, B.; Chen, X.; Shang, J.; Lu, W. D.; Wu, Y.; Li, R. W., An optoelectronic resistive switching memory with integrated demodulating and arithmetic functions. *Adv. Mater.* **2015,** *27*, 2797-2803.

(4) Lei, S.; Wen, F.; Li, B.; Wang, Q.; Huang, Y.; Gong, Y.; He, Y.; Dong, P.; Bellah, J.; George, A., Optoelectronic memory using two-dimensional materials. *Nano Lett.* **2015,** *15*, 259-265.

(5) Kim, G.; Cho, H. J.; Sheu, Y.-M.; Ohta, H., Electrical, Optical and Thermal Transport Properties of Oxygen Deficient Amorphous WO_x ($2.5< x< 3$) Films. *J. Phys. Chem. C* **2019,** *123*, 15419-15424.

(6) Liu, D.; Wang, C.; Yu, Y.; Zhao, B.-H.; Wang, W.; Du, Y.; Zhang, B., Understanding the nature of ammonia treatment to synthesize oxygen vacancy-enriched transition metal oxides. *Chem* **2019,** *5*, 376-389.

(7) Lim, J. S.; Lee, J.; Lee, B. J.; Kim, Y.-J.; Park, H.-S.; Suh, J.; Nahm, H.-H.; Kim, S.-W.; Cho, B.-G.; Koo, T. Y., Harnessing the topotactic transition in oxide heterostructures for fast and high-efficiency electrochromic applications. *Sci. Adv.* **2020,** *6*, eabb8553.

(8) Biswas, A.; Yang, C.-H.; Ramesh, R.; Jeong, Y. H., Atomically flat single terminated oxide substrate surfaces. *Prog. Surf. Sci.* **2017,** *92*, 117-141.

(9) Nagashima, K.; Yanagida, T.; Tanaka, H.; Kawai, T., Stress relaxation effect on transport properties of strained vanadium dioxide epitaxial thin films. *Phys. Rev. B* **2006,** *74*, 172106.

(10) Cao, J.; Ertekin, E.; Srinivasan, V.; Fan, W.; Huang, S.; Zheng, H.; Yim, J.; Khanal, D.; Ogletree, D.; Grossman, J., Strain engineering and one-dimensional organization of metal–insulator domains in single-crystal vanadium dioxide beams. *Nat. Nanotechnol.* **2009,** *4*, 732-737.

(11) Krüger, P.; Koutiri, I.; Bourgeois, S., First-principles study of hexagonal tungsten trioxide: Nature of lattice distortions and effect of potassium doping. *Phys. Rev. B* **2012,** *86*, 224102.

(12) Lee, Y.; Lee, T.; Soon, A., Polytypism in hexagonal tungsten trioxide: Insights from ab initio molecular dynamics simulations. *J. Phys. Chem. C* **2018,** *122*, 21644-21650.

(13) Palermo, V.; Kinloch, I. A.; Ligi, S.; Pugno, N. M., Nanoscale mechanics of graphene and graphene oxide in composites: a scientific and technological perspective. *Adv. Mater.* **2016,** *28*, 6232-6238.

(14) Han, J.; Pugno, N. M.; Ryu, S., Nanoindentation cannot accurately predict the tensile strength of graphene or other 2D materials. *Nanoscale* **2015,** *7*, 15672-15679.

(15) Soma, T.; Yoshimatsu, K.; Ohtomo, A., Epitaxial growth of hexagonal tungsten bronze Cs_xWO_3 films in superconducting phase region exceeding bulk limit. *Appl. Phys. Express* **2016,** *9*, 075801.

(16) Wu, P. M.; Ishii, S.; Tanabe, K.; Munakata, K.; Hammond, R.; Tokiwa, K.; Geballe, T.; Beasley, M., Synthesis and ionic liquid gating of hexagonal WO_3 thin films. *Appl. Phys. Lett.* **2015,** *106*, 042602.

(17) Yang, Q.; Cho, H. J.; Jeen, H.; Ohta, H., Macroscopic visualization of fast electrochemical reaction of $SrCoO_x$ oxygen sponge. *Advanced Materials Interfaces* **2019,** *6*, 1901260.

(18) Lu, Q.; Yildiz, B., Voltage-controlled topotactic phase transition in thin-film $SrCoO_x$ monitored by in situ x-ray diffraction. *Nano Lett.* **2016,** *16*, 1186-1193.

(19) Lu, Q.; Chen, Y.; Bluhm, H.; Yildiz, B., Electronic structure evolution of $SrCoO_x$ during electrochemically driven phase transition probed by in situ X-ray spectroscopy. *J. Phys. Chem. C* **2016,** *120*, 24148-24157.

(20) Yang, Q.; Cho, H. J.; Jeen, H.; Ohta, H., Solid-state electrochemical redox control of the optoelectronic properties for $SrFeO_x$ thin films. *J. Appl. Phys.* **2021,** *129*, 215303.

(21) Kim, G.; Feng, B.; Sheu, Y.-M.; Cho, H. J.; Ikuhara, Y.; Ohta, H., Coexistence of High Electron Conduction and Low Heat Conduction in Tungsten Oxide Epitaxial Films with 1D Atomic Defect Tunnels. *ACS Appl. Electron. Mater.* **2020,** *2*, 2507-2513.

(22) Kim, G.; Feng, B.; Ryu, S.; Cho, H. J.; Jeen, H.; Ikuhara, Y.; Ohta, H., Anisotropic Electrical Conductivity of Oxygen-Deficient Tungsten Oxide Films with Epitaxially Stabilized 1D Atomic Defect Tunnels. *ACS Appl. Mater. Interfaces* **2021,** *13*, 6864-6869.

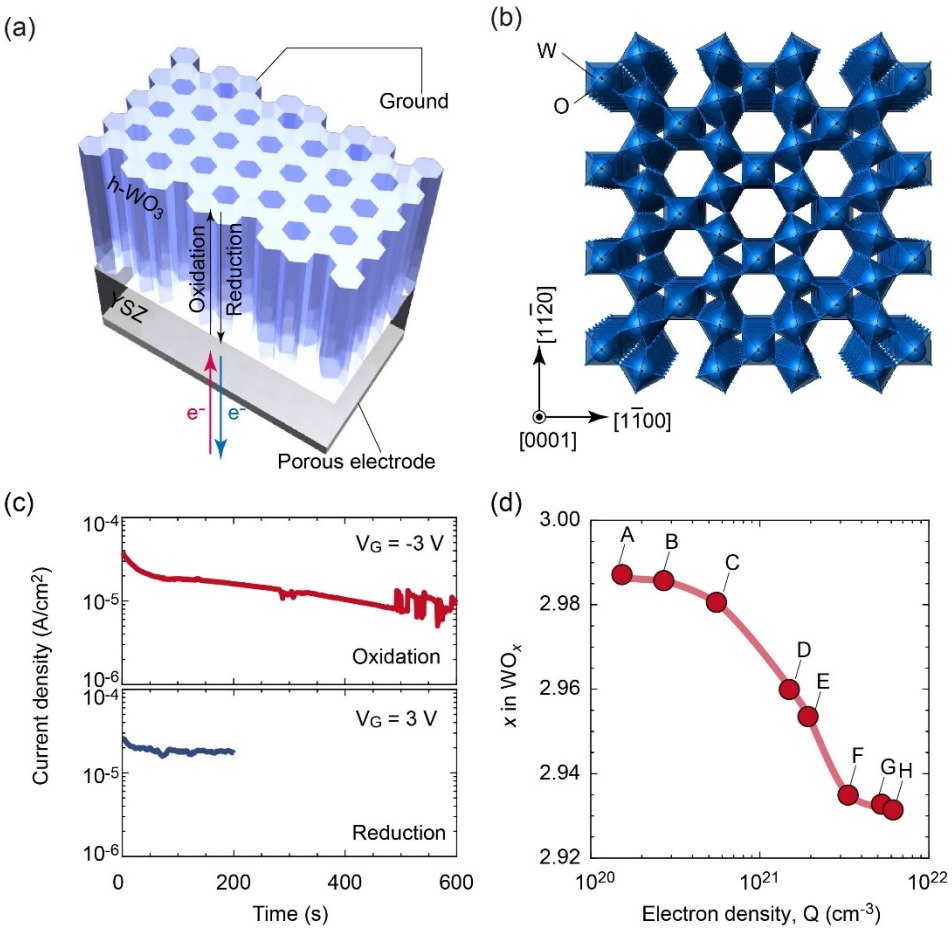

Figure 1. Solid-state electrochemical redox treatment of a h-WO_x epitaxial film. (a) Schematic illustration of the solid-state electrochemical cell composed of h-WO_3/YSZ substrate. (b) Honeycomb lattice of h-WO_3 crystal with periodic holes along the *c*-axis. (c) Change in the current density through the h-WO_3/YSZ bilayer at 300 °C in air. (d) Change in the oxygen content *x* in h-WO_x as a function of the electron density during the electrochemical reduction treatment.

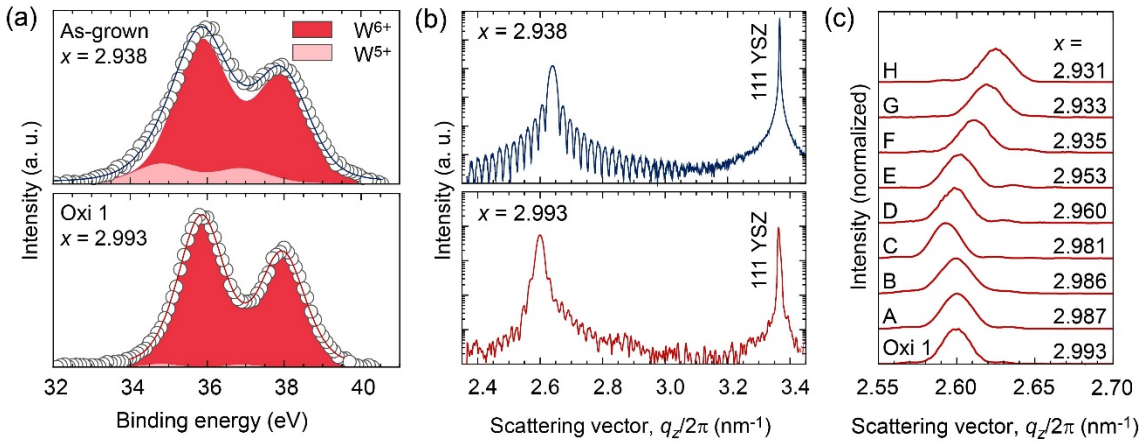

Figure 2. **Cross-plane crystal lattice of the h-WO_x films.** (a) XPS spectra of (upper) as-grown and (lower) electrochemically oxidized h-WO_x films. The x values in WO_x were determined as 2.938 (as-grown) and 2.993 (oxidized). (b) Out-of-plane XRD patterns of (upper) as-grown and (lower) electrochemically oxidized h-WO_x films. Intense diffraction peak of 0002 h-WO_x is seen together with 111 YSZ both as-grown and oxidized films. Further, Pendellösung fringes are seen around the diffraction peak of 0002 h-WO_x, indicating strong orientation of the films. (c) Change in the out-of-plane XRD patterns of 0002 h-WO_x (linear scale) with x in the electrochemically reduced WO_x films.

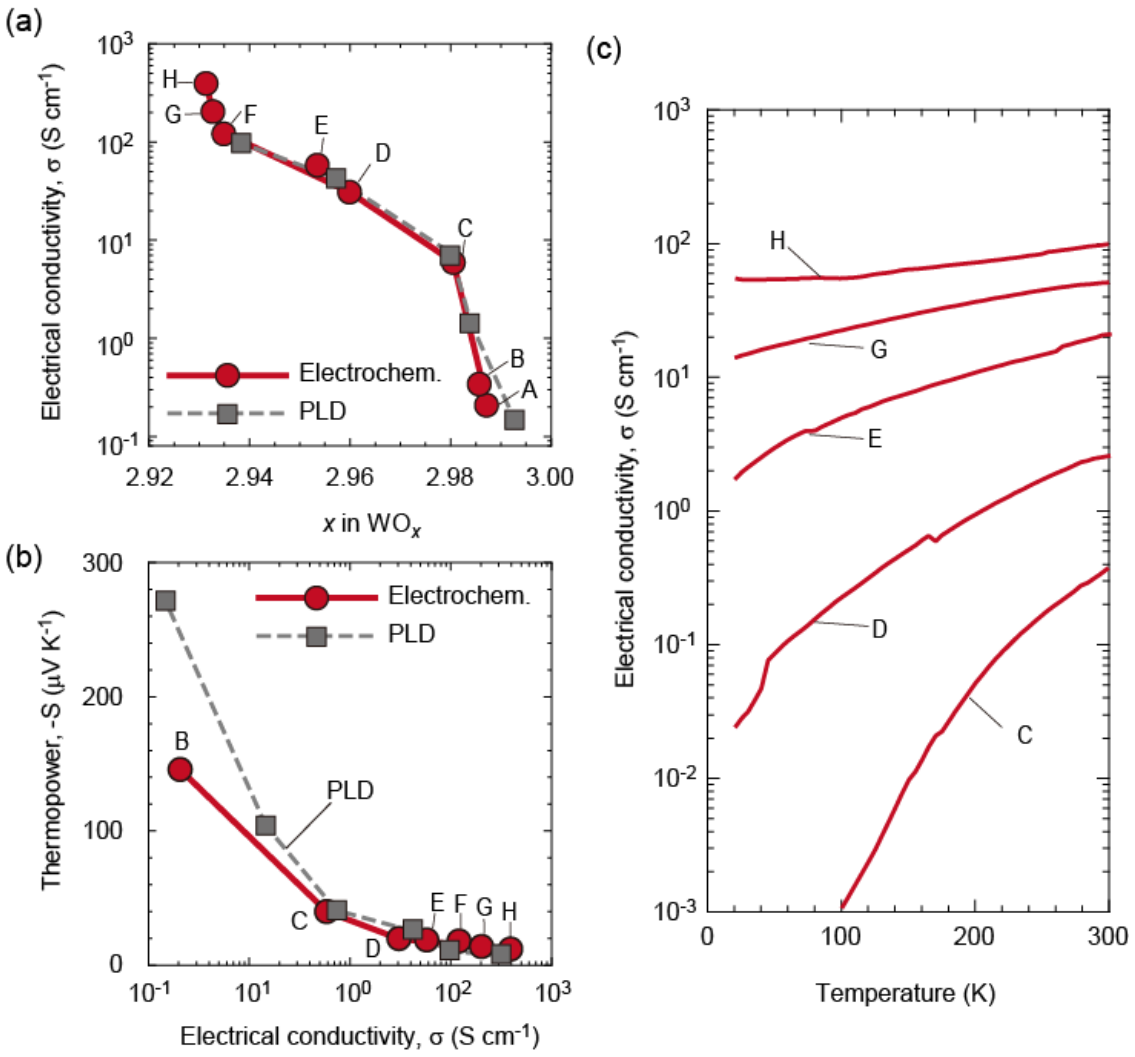

Figure 3. **Electronic properties.** (a) Electrical conductivity (RT), (b) thermopower (RT), and (c) temperature dependence of the electrical conductivity for the electrochemically reduced WO_x films. Gray solid lines in (a) and (b) indicate the electrical conductivity and the thermopower of the h-WO_x epitaxial films by the PLD method with modulated oxygen pressure during the film growth, respectively. Plots (electrochemical redox results) reproduce the PLD data very well, suggesting the crystal lattice of h-WO_x film was not destroyed during the redox treatment. (c) Temperature dependence of electrical conductivity of the h-WO_x films. The electrical conductivity is systematically controlled.

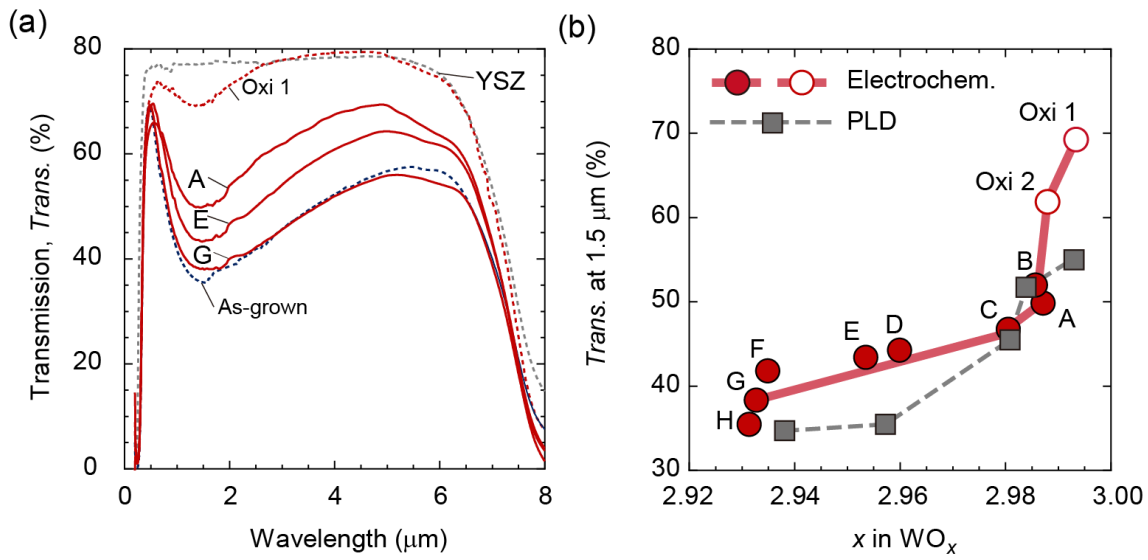

Figure 4. **Optical property** (a) Optical transmission spectra of the *c*-axis oriented h-WO_x film epitaxially grown on (111) YSZ substrate after the electrochemical reduction treatment. Optical transmission spectrum of YSZ substrate and as-grown h-WO_x film are shown for comparison. There is a tiny free electron absorption peaking around 1.5 μm in the fully oxidized film (Oxi 1). The absorption band increases with increasing the reducing degrees and it approaches that of the as-grown sample. (b) Optical transmission at 1.5 μm in wavelength as a function of x in WO_x. Gray solid lines indicate optical transmission at 1.5 μm in wavelength of the h-WO_x epitaxial films by the PLD method with modulated oxygen pressure during the film growth.

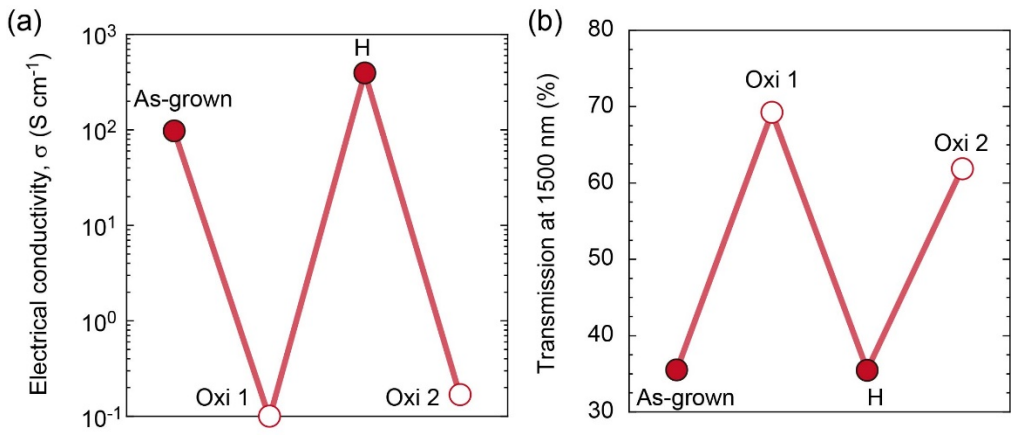

Figure 5. Reversible redox modulation of optoelectronic properties of the h-WO_x epitaxial films. (a) Electrical conductivity and (b) optical transmission at 1.5 μm in wavelength for the h-WO_x epitaxial films. Upon reversible electrochemical redox treatment, the electrical conductivity is controlled from ~100 S cm^{-1} to ~0.1 S cm^{-1}, and the optical transmission at 1.5 μm in wavelength is controlled in the range of 35 − 70%.